

Optimizing PTP Motions of Industrial Robots through Addition of Via-points

Zygimantas Ziaukas, Kai Eggers, Jens Kotlarski and Tobias Ortmaier

Institute of Mechatronic Systems, Gottfried Wilhelm Leibniz Universität Hannover, Appelstr. 11a, Hanover, Germany

Keywords: Energy Savings, Energy Efficiency, Time Savings, Efficient Trajectory, Reduced Moment of Inertia, Industrial Robotics.

Abstract: This paper presents how the addition of via-points can improve the state-of-the-art trajectory planning towards lower energy consumption and/or lower travel time. In contrast to existing approaches using trajectory interpolation methods like B-splines, exclusively standard commands of commonly available robotic systems are used in order to get practicable results. The system's energy demand for a given trajectory is determined based on a model of system energy characterized by low complexity. Trajectory profiles are obtained from original robot trajectory planning by using hardware in the loop. Therefore, results can directly be formulated in machine code. Experimental results demonstrate the effectiveness of the proposed approach. Depending on the given task, energy savings up to 17.3 % at equal travel time and time savings up to 13.3 % compared to initial PTP motion are possible. The approaches presented are applicable to any robotic application that utilizes PTP motions, e. g. pick-and-place or spot welding tasks.

1 INTRODUCTION

Sales of industrial robots reached an all time high of 248,000 units sold in 2015 worldwide, increasing by about 12 % compared to the previous year (IFR, 2016). For the future, ongoing significant growth is expected. A rising degree of automation leads to an increase of overall energy consumption. On the one hand, manufacturers aim to reduce production costs to stay competitive in the dynamic global market. On the other hand, sustainability becomes more and more a matter of interest regarding the companies' image and the requirement to meet legal regulations.

Earlier works mainly focus on optimizing cycle times, as manufacturers seek to maximize their production output and, therefore, their sales volume (Vergnano et al., 2012),(Riazi et al., 2015),(Wigstrom et al., 2013). Nowadays, due to the aforementioned reasons, the reduction of energy consumption, becomes more relevant (Brossog et al., 2015).

In this paper, we present methods to reduce energy consumption as well as travel time for robotic PTP motions. Both criteria are the main target of most optimization approaches. Thanks to the generic optimization method, travel time as well as energy consumption can be considered independently or at the same time.

Several methods for the reduction of either energy consumption or travel time have been presented. In (Vergnano et al., 2012), the view is expanded on multi-robot systems. Scheduling is optimized using idle times to slow down operations with the highest energy consumption. Furthermore, it was recognized that different operations have different optimization possibilities. Our research confirms these findings. Similar methods can be found in e.g. (Riazi et al., 2015) and in (Wigstrom et al., 2013) where additionally the movements of the individual robots are optimized.

Towards reducing energy consumption of individual robots' PTP motions, an approach with asynchronous fly-by in joint space is presented in (Meike and Ribickis, 2011). Unnecessary acceleration and deceleration phases, identified by an algorithm, are diminished and motion profiles are smoothed by using cubic B-splines for trajectory interpolation. In (You et al., 2011), cubic spline interpolation is modified, resulting in energy and travel time reduction.

The opportunity of using recuperated energy from deceleration phases via DC-Bus is presented in (Hansen et al., 2013). Either direct usage in times of simultaneous acceleration and deceleration of different axes or energy storage, e.g. in capacitors, is conceivable. This approach is continued in (Hansen

et al., 2015). Further approaches to reduce energy consumption for PTP motions are presented in (Paes et al., 2014),(Mohammed et al., 2014).

Some of the previously mentioned works also include a possible reduction of travel time by replacing the objective function. An early approach towards time optimization is presented in (Bobrow, 1988). Cartesian trajectories are represented by B-Splines and adjusted in a time-optimal way.

Moreover, in (Gleeson et al., 2015), continued in (Gleeson et al., 2016), trajectories are optimized and code for robot control is generated automatically. By setting via-points and corresponding zone radii which specify the maximum approximation of the via-point and assure a collision free trajectory, the time optimal trajectory is defined. In (Gattringer et al., 2013), an approach of directly manipulating a PTP trajectory's joint angle functions over time is introduced.

The methods we propose are based on a model of system energy which, in contrast to the present trend of research (Meike and Ribickis, 2011),(Hansen et al., 2012), is more simple. The survey in (Brossog et al., 2015) shows that current research in this field develops towards more detailed energy models, including power losses such as core losses, windage and friction losses, stator and rotor losses, stray load losses, inverter, and rectifier losses. For optimization methods like ours, this level of detail is inefficient. We intend to present a sufficient energy model for serial kinematic industrial robots, based on which a practicable optimization approach for the reduction of energy consumption can be applied and customized to commercial robot control systems. Supplementally, we show that our approach can be modified easily to meet different criteria. Exemplary, travel time is considered.

Our model is described and validated in section 2. Standard PTP trajectory planning approaches, implemented in modern robot controls, and our methods of modifying them in order to reduce energy consumption and/or travel time are presented in section 3. Finally, results and conclusions are presented in sections 4 and 5.

Additionally, in section 5.2 we introduce an future works approach of optimizing trajectories by adding via-points to initial PTP motions with minimized moment of inertia. Already in (Geering et al., 1985) it is mentioned that minimization of moment of inertia with respect to revolute joints leads to time-optimal trajectories. This method has significant advantages regarding computation time needed, as the complexity of the cost function is further reduced and even less knowledge of the system is required.

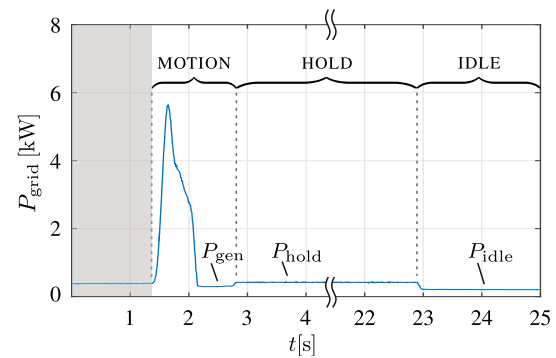


Figure 1: Typical power consumption measurement for an industrial robot in different operating phases.

2 MODEL OF SYSTEM ENERGY

Comprehensive energy demand modelling approaches for mechatronic systems have been presented in earlier publications (Hansen et al., 2013; Pellicciari et al., 2013). However, the proposed model is specifically designed for industrial robots, which enables significant model complexity reductions without perceptible changes in accuracy. This leads to advantages in feasibility, computation time, and system identification effort. Assuming that the parameters of the inverse dynamics model are known, the presented power model uses only three additional parameters that can be identified in a single measurement. The correct simulation and comparison of the energy consumption for different travel times requires a model representing the consumption while in motion as well as in standstill. In order to clarify the different power consumption phases, a typical power measurement for a PTP motion is shown in Figure 1. The operational state can be divided into three different phases:

- MOTION means that the robot is currently moving,
- HOLD describes a robot in active control with lifted holding brakes, while
- IDLE signifies that the holding brakes have been applied.

The causes for the power consumption in the different phases are explained in section 2.1, along with the identification of the required parameters. The modelling of the motion-dependent power consumption is formulated in section 2.2. Validation measurements are presented in section 2.3.

2.1 Operating Phases

The power consumption during the different operating phases can be explained by consideration of a

simplified electrical substitute circuit diagram (Figure 2). During the MOTION phase, the power consumption depends on the robot's mechanical power demand $P_{\text{mech},i}$ that is induced by the given motion. A detailed description of the modelling approach for this particular term can be found in section 2.2. The sum of mechanical powers is represented by an auxiliary variable P_{DC} that characterizes the power flow within the DC bus. Since most state-of-the-art robot controls are not able to recuperate, excess power P_{R} is dissipated through a brake resistor. All further DC bus losses are summarized as a constant loss power $P_{\ell,\text{DC}}$. Constant losses on the grid side are split into two groups: the power P_{brk} is required to keep the brakes lifted while $P_{\ell,\text{grid}}$ summarizes the constant losses of all peripheral components (e.g. controller, cooling fans, IO modules, sensors, etc.).

During the IDLE phase, all the components on a 600 V level are inactive and the holding brakes are applied. Hence, the measurable power P_{idle} equals $P_{\ell,\text{grid}}$. In the HOLD phase, the power demand is induced by the constant losses on the grid side, on the DC side, and by the brake lifting power:

$$P_{\text{hold}} = P_{\ell,\text{grid}} + P_{\ell,\text{DC}} + P_{\text{brk}}. \quad (1)$$

The power consumption for the static holding is not considered separately. It is instead included in the constant DC losses $P_{\ell,\text{DC}}$. The dependency on the robot configuration is neglected: measurements have shown a maximum deviation of P_{hold} of approx. 10% for the KUKA KR 16 and 5% for the KUKA KR 210 for the most extreme poses (see section 2.3 for the test bed description). The influence for the KR 210 is lower due to its counterbalancing system. However, with regard to the robots' peak powers of approx. 8 kW (KR 16, see Figure 4) and 20 kW (KR 210, see Figure 5), the deviation comes down to less than 0.01% in each case.

The utilization of substitute powers for various losses is a major change in comparison to existing approaches (Hansen et al., 2013; Pellicciari et al., 2013). Industrial robots usually feature backlash free gears with high friction. Hence, the mechanical losses clearly exceed the electrical ones. Therefore, the proposed simplifications only have a minor impact on the grid power consumption (see also section 2.3). The main advantage of this approach is the significant reduction of required parameters which enables the model for application on an industrial level.

2.2 Motion-dependent Power Consumption

This section focuses on the calculation of the motion-dependent power consumption. Assuming that a tra-

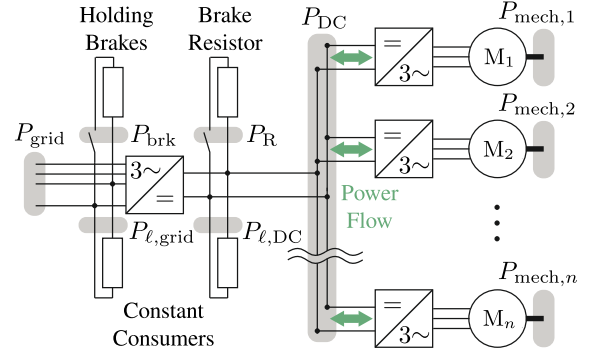


Figure 2: Electrical substitute circuit diagram for an industrial robot.

jectory of an industrial robot is predefined, the calculation of the system power demand starts with determining the motor torques $\tau(t)$. In general, the model for inverse dynamics is given by

$$\tau(t) = \text{diag}\left(\frac{1}{u_{G,1}}, \dots, \frac{1}{u_{G,n}}\right)(M(q)\ddot{q} + c(q, \dot{q}) + g(q) + h(q, \dot{q})), \quad (2)$$

where q, \dot{q}, \ddot{q} are time-dependent joint angles, velocities, and accelerations given by the trajectory planning algorithm. The term $u_{G,i}$ represents the gear factor for joint i while the vector τ contains the respective motor torques τ_i . M contains moments of inertia, c Coriolis effects, and g gravitational effects. h summarizes non-linear effects which in our regarded case is merely friction. In (Hamon et al., 2010), a commonly used friction model including Coulomb friction and viscous damping (coefficients $f_{c,i}$ and $f_{v,i}$, respectively) is presented. It is applied for this model, expressing friction torque $\tau_{f,i}$ for joint i as

$$\tau_{f,i}(t) = h_i(t) = f_{c,i} \text{sign}(\dot{\omega}_i(t)) + f_{v,i} \dot{\omega}_i(t), \quad (3)$$

where ω_i is the angular motor velocity of motor i which can be determined as

$$\omega_i(t) = u_{G,i} \dot{q}_i(t). \quad (4)$$

Most robotic manufacturers utilize a model of the inverse dynamics within the robot control system for implementation of feed forward control. Thus, it can be assumed that the system friction parameters are known. If not, they can be obtained using established identification methods (Johnson and Lorenz, 1992). Equations 2 and 4 are used to obtain the mechanical power $P_{\text{mech},i}(t)$ for each motor i :

$$P_{\text{mech},i}(t) = \tau_i(t) \omega_i(t). \quad (5)$$

The total DC bus power P_{DC} is obtained by summing up the mechanical power of the n individual motors:

$$P_{\text{DC}}(t) = \sum_{i=1}^n P_{\text{mech},i}(t). \quad (6)$$

For state-of-the-art industrial robots, the DC bus features a capacitor that is usually dimensioned to smoothen the rectified voltage, not to buffer excess energy in generator operation phases. Therefore, the capacity is neglected. However, it can be implemented according to (Hansen et al., 2012) if desired. Further, the rectifiers in industrial robot cabinets are usually not able to recuperate. Hence, negative values for P_{DC} need to be partly corrected. The excess power in generator operating phases can cover the constant losses within the DC bus, but the grid side losses will remain. The remaining power consumption is marked as P_{gen} in Figure 1. This behaviour is considered as follows:

$$\begin{aligned}
 P_{DC}(t) + P_{\ell,DC} &\geq 0: \\
 P_{grid}(t) &= P_{DC}(t) + P_{\ell,DC} + P_{\ell,grid} + P_{brk}, \\
 P_R(t) &= 0, \\
 P_{DC}(t) + P_{\ell,DC} &< 0: \\
 P_{grid}(t) &= P_{gen} = P_{\ell,grid} + P_{brk}, \\
 P_R(t) &= -(P_{DC}(t) + P_{\ell,DC}),
 \end{aligned}$$

where $P_R(t)$ is the power dissipated via the brake resistor. The time integral of the grid power demand over trajectory time (from t_{start} to t_{end})

$$E_{grid} = \int_{t_{start}}^{t_{end}} P_{grid}(t) dt \quad (7)$$

equals the grid energy demand of the system for a given trajectory.

2.3 Validation

In order to demonstrate its portability, the model is applied to and parameterized for two robots of different sizes, namely a KUKA KR 16 and a KUKA KR 210 with respective payloads of 16 kg and 210 kg. The test setup for the validation is shown in Figure 3. The grid power is measured using a Yokogawa WT 3000 precision power analyzer. The robots are equipped with a test weight of 15 kg and 200 kg.

The Figures 4 and 5 show the measured as well as the simulated power demand and the grid energy demand for both robots. The validation trajectory consists of five PTP motions, separated by one-second pauses. The resulting grid energy demand for the KR 210 is slightly overestimated by the simulation by +5.3%. At about 10 s, the power demand differs a little bit more extreme than for the other motions. This might occur due to inaccuracies in the robot control's inverse dynamic model for this exact movement.

For the KR 16, the simulation provided an even lower deviation of 1.2% for the given trajectory. Further measurements with varying trajectories delivered

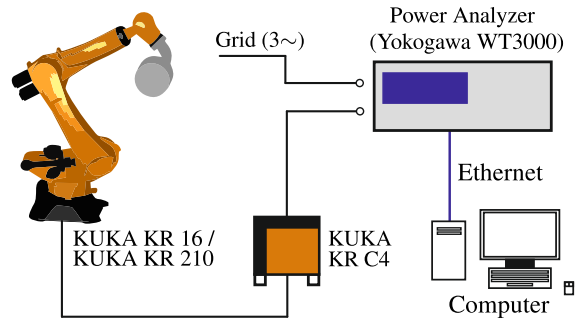


Figure 3: Test setting for validation trajectory measurement; figures are properties of the respective manufacturers.

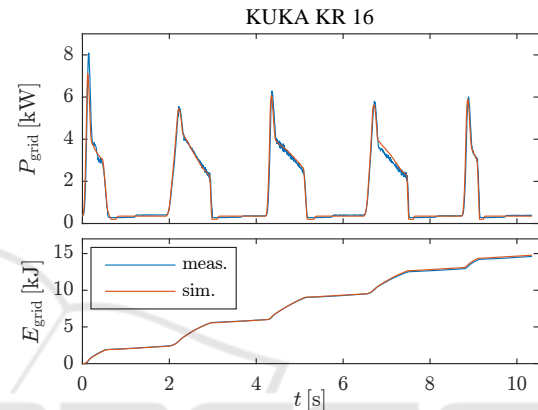


Figure 4: Measured and simulated power demand for the KUKA KR 16.

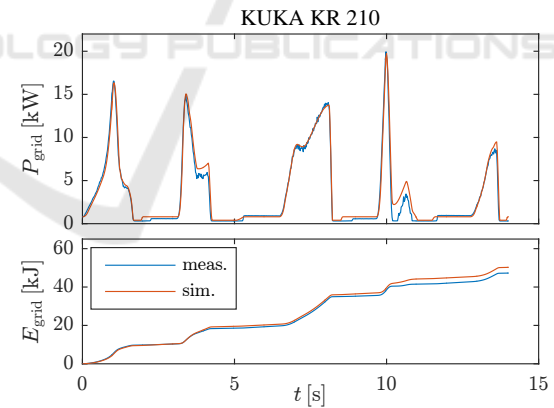


Figure 5: Measured and simulated power demand for the KUKA KR 210.

comparable results with an error within approx. $\pm 5\%$. The validation results show that the model with the proposed complexity reductions, in contrast to increasingly complex models in the current development of research, adequately depicts the real system's grid power and energy demand.

While different simplifications have been introduced for the modelling of the electrical part of the drive system, it is important to reach a high accuracy

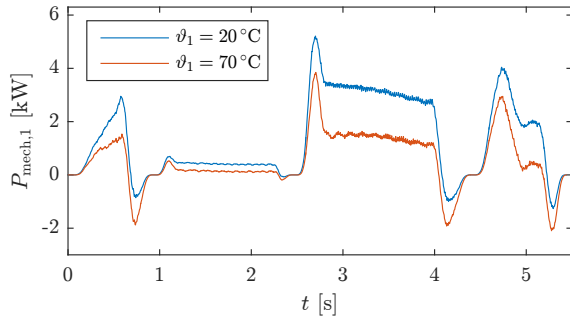


Figure 6: Mechanical power comparison for axis $i = 1$ at different motor temperatures based on measured (traced) values for τ_1 and ω_1 .

for the calculation of the mechanical power. Although there is a strong dependency between robot temperature and its power demand, previous works often neglect this. While (Brossog et al., 2015), (Meike et al., 2014) consider the robot temperature, only the temperature dependencies of motor resistors are taken into account.

Figure 6 demonstrates the impact of the robot (i. e. motor) temperature on the mechanical power. The values are based on the traced values at a KR 210 using its internal sensors. While the motor temperature ϑ_i does not equal the gear temperature, it sufficiently displays the robot's thermal state. The measured grid energy consumption for the same motion at different temperatures is shown in Figure 7. It becomes obvious that a consideration of the temperature within the model is inevitable. Therefore, the model should either utilize temperature-dependent friction parameters or they need to be identified for a task-specific thermal state. For this paper, the friction parameters were identified for motor temperatures of 60 °C. Unless stated otherwise, all presented measurements and results refer to this operating point.

3 OPTIMIZATION APPROACH

The following section describes state-of-the-art trajectory planning implemented in several standard industrial robot control systems. Following, the proposed approach to modify trajectories towards less energy consumption is introduced. Additionally, optimization of travel time is considered. Furthermore, the optimization method including its cost functions and boundaries are presented.

3.1 Standard Trajectory Planning

A common solution for PTP trajectory planning is based on trapezoidal acceleration profiles with syn-

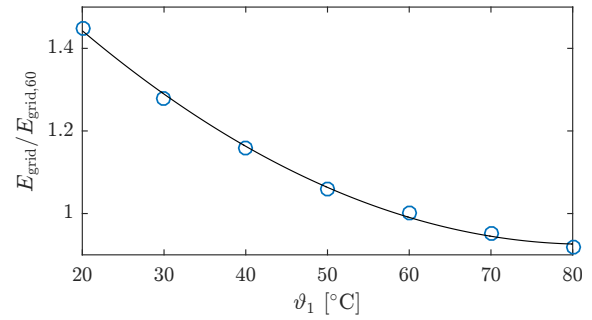


Figure 7: Dependency of grid energy demand E_{grid} on temperature normalized to the grid energy demand $E_{\text{grid},60}$ at 60 °C motor temperature.

chronously moving axes (Biagiotti and Melchiorri, 2008). This results in continuous joint angle, velocity, and acceleration functions, but in a non-continuous jerk function. However, the actual acceleration functions of modern robot controls differ from strict trapezoidal profiles to further improve travel time. Acceleration is constrained by the maximum torque limits of the axes (Costantinescu and Croft, 2000). This leads to at least one axis reaching its torque limit, as shown in the results section. All axes move synchronously.

3.2 Trajectory Modification by adding Via-Points

By adding via-points we are able to modify a given trajectory towards optimized energy consumption and/or travel time. The advantage of this method, in contrast to previous works using spline interpolation such as (Meike and Ribickis, 2011), (You et al., 2011), (Hansen et al., 2012), is the simple implementation to commercial robot controls. The method exclusively utilizes standard control commands. Initially, this seems paradoxical since adding via-points seem like a detour on the way from starting to final configuration. However, if the via-points are placed in an certain position, a configuration with reduced moments of inertia $M(\mathbf{q})$ can result. According to (2), a reduction of $M(\mathbf{q})$ can be exploited to

- increase joint acceleration at equal joint torque or
- decrease joint torque at equal joint acceleration.

Possible benefits are pointed out in the following two scenarios: Assuming the user wants to lower energy consumption for a given PTP motion without changing the travel time, lower joint torques can decrease the total energy demand, whereas maintaining equal acceleration keeps the travel time constant.

Alternatively, the user wants to lower travel time for a given PTP motion. This could be accomplished

by increasing joint acceleration, which is limited by maximum joint torque, as described in section 3.1. Thanks to the reduced moment of inertia in via-point configuration compared to the initial trajectory, acceleration can be increased without exceeding the torque limits.

The addition of via-points can also desynchronize the axes' movement. Non-synchronously moving axes allow the usage of recuperated energy from deceleration phases through DC-bus linkage, which leads to a reduction of dissipated energy and, therefore, to a higher overall energy efficiency. Figure 2 shows the corresponding energy flows.

Any number of via-points can be added to the initial trajectory. However, in order to assure a simple understanding we present our methods and results based on the addition of one via point. Note that more via-points increase the computational expense due to the increased dimension of the optimization parameter vector.

Furthermore, apart from the optimization of energy consumption, other targets can be considered by replacing the cost function. As the optimization of travel time is often addressed in previous works, it is additionally considered in this paper.

3.3 Optimization Method

The initial trajectory with synchronously moving axes as described in section 3.1 is programmed in robot control as shown in Figure 8. It represents a PTP motion from starting joint angle configuration q_s to end configuration q_e . Velocity and acceleration are set to maximum (100%) which are the default values in most common robot control systems.

The optimization target is set by defining the cost function. Basically, any type of cost function can be formulated. Following, we focus on reduction of energy consumption and additionally travel time.

3.3.1 Optimization of Energy Consumption

The optimization parameter vector

$$p_e = (\underbrace{p_1, p_2, \dots, p_n}_{p_{e, \text{joint config}}}, v, a)^T \quad (8)$$

contains all n joint angles of the via-point added to the initial trajectory between start and end configuration, velocity v , and acceleration a . Velocity and acceleration are expressed in percentage of the respective set maximums.

The initial as well as the temporary trajectories of iteration steps, are generated using original trajectory planning of the robot control system. This is realized

```

1 for i=1 to 6
2   $acc_axis[i]=100  initial accel. and velocity
3   $vel_axis[i]=100  settings in %
4 endfor
5
6
7
8 Points for PTP motion in joint space
9 PTP {A1 qs,1, A2 qs,2, A3 qs,3, A4 qs,4, A5 qs,5,
      A6 qs,6}
10
11 PTP {A1 qe,1, A2 qe,2, A3 qe,3, A4 qe,4, A5 qe,5,
      A6 qe,6}
    
```

Figure 8: Trajectory Source Code in Kuka Robot Language.

by including hardware in the loop of optimization. This method of trajectory generation automatically satisfies all constraints like maximum motor torques, maximum gear torques, maximum joint velocities set by the robot manufacturer. It also allows to simply implement the optimized trajectory in the robot control by using standard commands. In contrast, if the trajectory is interpolated e.g. using B-splines, this becomes more problematic. The resulting joint angles $q(t)$, velocities $\dot{q}(t)$, and accelerations $\ddot{q}(t)$ are then used to calculate the energy consumption of the motion as described in section 2.2. The optimization problem is formulated as a minimization of total energy demand

$$p_e^* = \arg \min_{p_e} (E_{\text{grid}}(q_s, p_e, q_e)), \quad (9)$$

where p_e^* is the optimal parameter vector. All parameters' upper and lower bounds are

$$q_{i, \min} \leq p_i \leq q_{i, \max} \quad \forall i = 1 \dots n, \quad (10)$$

$$0\% \leq v \leq 100\%, \quad (11)$$

$$0\% \leq a \leq 100\%, \quad (12)$$

where limits to p_i originate from kinematic constraints, preventing the robot from colliding with obstacles or itself. Additionally, a non-linear constraint

$$t_{\text{temp}} \leq t_{\text{thr}} \quad (13)$$

is implemented to ensure that the travel time of the temporary optimized trajectory t_{temp} in each iteration does not impair the threshold travel time t_{thr} . Threshold travel time commonly is the travel time of the initial trajectory t_{init} .

3.3.2 Optimization of Travel Time

In contrast, if the target is to optimize the travel time, the optimization parameter vector slightly changes to

$$p_t = (p_1, p_2, \dots, p_n)^T. \quad (14)$$

```

1 for i=1 to 6
2 $acc_axis[i]=a*  opt. acceleration and velocity
3 $vel_axis[i]=v*  settings in %
4 endfor
5
6 $apo.cptp=100  via-point approx. set to max.
                  only affects points between
                  start and end configuration
7
8 Points for PTP motion in joint space
9 PTP {A1 qs,1, A2 qs,2, A3 qs,3, A4 qs,4, A5 qs,5,
      A6 qs,6}
10 PTP {A1 p1*, A2 p2*, A3 p3*, A4 p4*, A5 p5*,
      A6 p6*} [c-tp]
11 PTP {A1 qe,1, A2 qe,2, A3 qe,3, A4 qe,4, A5 qe,5,
      A6 qe,6}
    
```

Figure 9: Optimized Trajectory Source Code.

In this case, the optimization process has no influence on velocity and acceleration settings, as minimal travel time arises from both variables set to their maximum of

$$v = v_{\max} = 100\%, \quad (15)$$

$$a = a_{\max} = 100\%. \quad (16)$$

Again, trajectories are generated utilizing the original trajectory planning from the robot control. This includes calculation of travel time t_{trav} . The resulting cost function is

$$p_t^* = \arg \min_{p_t} (t_{\text{trav}}(q_s, p_t, q_e)) \quad (17)$$

and does not include the model of system energy in section 2. Parameter bounds are the same as defined in (10), respectively.

Additional non-linear constraints can be considered to further tune the trajectory according to required characteristics. For instance, in order to restrict the deviation of the optimized trajectory from the initial, a constraint to ensure the optimized trajectory stays in bounds of a tube with a defined radius around the initial trajectory can be used (Hussong and Heimann, 2007).

Analogically, any kind of restriction can be considered, however, additional non-linear constraints can lead to less flexibility for the optimization which leads to less advance in performance. Improvement possibilities depend on the initial trajectory and the workspace circumstances.

3.3.3 Optimization Procedure

The non-linear optimization problem is solved using an active-set algorithm. The starting point for optimization is set in the middle (in joint space) between

start and end configuration

$$p_{e,\text{joint config.}}^{\text{start}} = p_t^{\text{start}} = \frac{q_s + q_e}{2}. \quad (18)$$

The resulting optimal parameter vector is then used to optimize the robot control program. In case of the addition of multiple via-points, starting points are equidistantly distributed.

The whole optimization process runs automatically. A robot control program on a KUKA KR C4 is read and relevant information is extracted. Then, the actual optimization process is performed. Afterwards, a robot control program, including the added resulting via-points, is generated. Exemplary, a resulting optimized code for a single added via-point is shown in Figure 9.

4 RESULTS

This section presents optimization results for different PTP trajectories on the KUKA KR 210 industrial robot, shown in Figure 10. The model of system energy in section 2 and the optimization method in section 3 are applied. All trajectories analyzed include an additional test load of 200 kg mounted at the robot's end-effector flange.

Furthermore, initial trajectories move with maximum velocity and acceleration, as it is a standard in industrial application to achieve minimum travel times.

Like many other high-payload robots, the KR 210 has a counterbalancing system between axis 1 and 2. This lowers high torque demands for axis 2 in

Table 1: Start and End Configurations (in Degrees) of the PTP Trajectories with Energy and Time Optimized Via-Points.

T1	q_s^T	= [0.0 -5.0 0.0 0.0 0.0 0.0]
	$q_{\text{via,e}}^T$	= [-2.2 -69.8 6.9 4.0 -67.9 1.4]
	$q_{\text{via,t}}^T$	= [-0.3 -69.9 -42.7 0.4 -105.8 0.0]
	q_e^T	= [0.0 -140.0 0.0 0.0 0.0 0.0]
T2	q_s^T	= [-150.0 -5.0 -90.0 -45.0 -50.0 -45.0]
	$q_{\text{via,e}}^T$	= [-18.6 -51.4 -15.2 74.1 65.8 25.6]
	$q_{\text{via,t}}^T$	= [-9.3 -39.9 -38.7 61.1 96.0 22.1]
	q_e^T	= [-150.0 -90.0 90.0 180.0 125.0 120.0]
T3	q_s^T	= [-55.0 -5.0 10.0 100.0 10.0 -40.0]
	$q_{\text{via,e}}^T$	= [-28.0 -39.0 -23.6 -21.1 125.0 54.2]
	$q_{\text{via,t}}^T$	= [-22.3 -53.1 -26.9 -40.1 55.0 5.3]
	q_e^T	= [15.0 -105.0 -60.0 -180.0 100.0 50.0]
T4	q_s^T	= [-165.0 -115.0 -110.0 -316.0 -114.0 -316.0]
	$q_{\text{via,e}}^T$	= [16.5 -55.1 27.2 -4.7 47.1 -10.6]
	$q_{\text{via,t}}^T$	= [17.2 -51.2 26.6 -13.5 6.4 -14.3]
	q_e^T	= [166.0 -9.0 111.0 319.0 115.0 319.0]

stretched configurations. The influence of the counterbalancing system on the robot is included in the dynamic model (Hansen et al., 2012).

Table 1 shows exemplary chosen PTP trajectories including their starting and ending configurations. The trajectories cover different motion characteristics, such as horizontal and vertical motion, a combination of both and an all axis motion from minimum to maximum joint angle limit.

Additionally, the axis configurations of optimized via-points $q_{e,via}^*$ and $q_{t,via}^*$ for energy-optimized PTP motions are presented. Associated velocity and acceleration values are $v_{T1} = 74.7\%$, $v_{T2} = 80\%$, $v_{T3} = 72\%$, and $v_{T4} = 80\%$, whereas acceleration stays at almost 100% for all four trajectories.

Table 2: Results for Energy and Time Optimized Trajectories. The Colors, Associated to Figure 10, Highlight the Results.

	Travel Time [s]	Energy Cons. [J]	Time-Opt. Slowed [J]
T1 _{init}	2.96	9733	
T1 _{opti.e}	2.96	8060 (-17.2%)	
T1 _{opti.t}	2.57 (-13.3%)	9476 (-2.6%)	8195 (-15.8%)
T2 _{init}	3.50	15005	
T2 _{opti.e}	3.50	12992 (-13.4%)	
T2 _{opti.t}	3.09 (-11.7%)	15751 (+5.0%)	13535 (-9.8%)
T3 _{init}	3.01	11769	
T3 _{opti.e}	3.01	9678 (-17.3%)	
T3 _{opti.t}	2.85 (-5.33%)	13841 (+17.7%)	11345 (-3.6%)
T4 _{init}	4.84	30268	
T4 _{opti.e}	4.84	26692 (-11.8%)	
T4 _{opti.t}	4.44 (-8.3%)	30251 (-0.1%)	27422 (-9.4%)

The resulting energy savings are summarized in Table 2. For the exemplary chosen trajectories, we achieve energy savings up to 17.3%.

In order to clarify the effects leading to the improvement, T1 is analyzed in detail. Figure 11 shows initial and energy-optimized joint motor torques of T1. As mentioned in 3.1, torque limited trajectory generation leads to at least one axis reaching its maximum torque limit. Even though only axis 2 is supposed to move, the other horizontal axes have to compensate torques due to moments of inertia, Coriolis and gravitational effects. For T1, axes 3 and 5 even reach their torque limits. The added via-point of the energy-optimized trajectory allows the axes torques to be lowered more quickly. Axes 2 and 5 cross the zero torque level approximately 0.4s earlier than the initial trajectory. Overall reduced torques lead to energy savings of 17.2%. Retardations are prevented due to the applied boundaries.

Alternatively, the cost function can be exchanged to minimize the travel time. Optimization of travel time is performed as an example for other optimization targets. Time savings up to approximately 13% are accomplished.

Initial and time-optimized joint velocities of T1 in Figure 11 allow for a closer look at the time optimization. Standard trajectory planning for a difference between start and end configuration in only one axis, in this case axis 2, results in a single movement of that axis. In contrast, the optimized trajectory shows an additional movement of the previously *passive* axes, especially the parallel ones. The additional motions lead to an optimized configuration regarding moments of inertia, Coriolis and gravitational effects. Regarding axis 2, this allows for a motion with increased velocity after reaching its peak at about 1.6s, leading to time savings of 13.3% and simultaneous energy savings of 2.6% as a side effect.

The time savings can then be used to reduce acceleration and/or velocity settings, leading to reduced energy consumption. Hence, resulting energy savings are included in Table 2. The energy savings of the time-optimal slowed down trajectory come close to the energy-optimized results, but do not reach those. However, for optimization of travel time no model of system energy is required.

5 CONCLUSION AND FUTURE WORKS

5.1 Conclusion

A new approach to automatically improve PTP motions of robotic systems using standard robot control has been presented. The proposed methods were successfully implemented on the KUKA KR 210. The resulting optimized source code differs from the initial one only by the added via-points which can be added using standard commands of common robot control systems.

Exemplary, in this paper the addition of one via-point is considered. In case of multiple via-points, the procedure is same. The initial multiple via-points are distributed equidistantly between start and end configuration, as described in section 3.3.3, and then all of them are optimized at the same time towards minimizing the respective cost function. Note that addition of multiple via-points increases the dimension of the parameter vector by six per additional via-point for a robot with $n = 6$ degrees of freedom which raises computational expenses. However, the optimized tra-

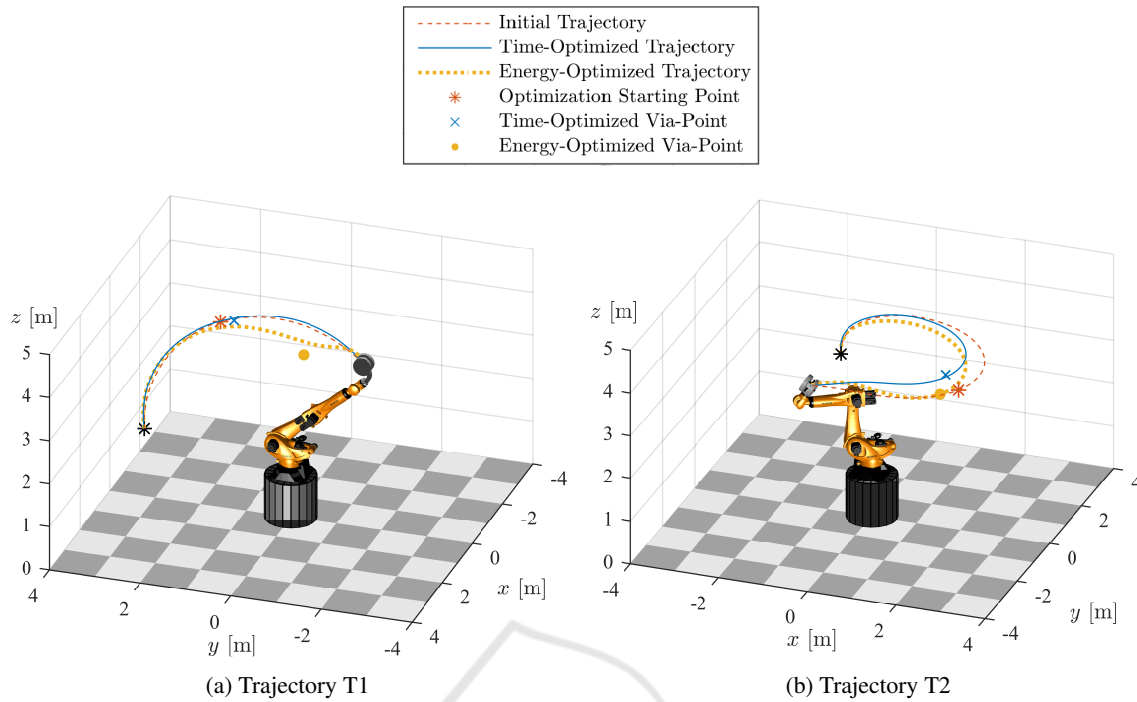


Figure 10: Exemplary Considered Trajectories T1 and T2.

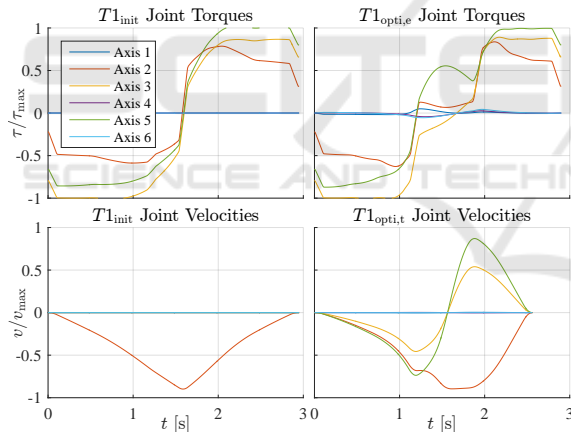


Figure 11: Comparison of Initial to Energy-Optimized Joint Motor Torques and Initial to Time-Optimized Joint Velocities of T1.

jectory could be specified more exactly which may lead to further optimization potential.

The via-point's configuration in joint space is calculated by formulating an optimization problem. Several optimization targets can be implemented by exchanging the cost function. In this paper we focus on reducing energy consumption and additionally consider optimization of travel time. Collision avoidance can be implemented by setting non-linear constraints.

In comparison to existing approaches, our model of system energy is more simple and requires less information of the system. However, it is suitable to

depict the energy demand of serial cinematic industrial robots and to be implemented for optimization procedure.

Based on the introduced model of system energy, the optimization problem to reduce energy consumption has been formulated. The experimental results have shown energy savings up to 17.3%.

In contrast, targeting to the optimization of travel time, a different cost function has been formulated. The implementation of this target has resulted in time savings up to 13.3%. These savings can also be used, to reduce energy consumption by decreasing acceleration and velocity settings on robot control. Hence, energy savings up to 15.8% are achieved.

Future works may focus on the addition of multiple via-points to the initial trajectory and on the evaluation of the results for a high number of different initial trajectories. Furthermore, the methods presented in this paper could be tested for different types of industrial robots.

5.2 Reduced Complexity Optimization Method

Reviewing the resulting trajectories of the presented approach lead to another method. Future works may focus on the direct minimization of moment of inertia. The complete model of system energy as well

as the inverse dynamics are highly complex and require a lot of system information. The advantages of reduced moments of inertia are explained in section 3.2. Following, an approach to optimize robot trajectories focusing on direct minimization of moment of inertia is proposed. In this case, the Cartesian inertia matrix \mathbf{M} needs to be calculated.

The cost function for this approach is

$$\mathbf{p}_{in}^* = \arg \min_{\mathbf{p}_{in}} (M_{(ax\ ax)}(\mathbf{p}_{in})), \quad (19)$$

where ax is the axis for which the moment of inertia is to be minimized, and parameter vector \mathbf{p}_{in} equals \mathbf{p}_t . The chosen axis depends on the initial trajectory. Initial and optimized robot control codes are programmed in the same manner as shown in section 3.3.

This approach comes along with some challenges. The cost function does not include any information about the resulting travel time or energy consumption. Therefore, an explicit target for the optimization can not be set.

Furthermore, reducing the moment of inertia is not suitable for all kinds of trajectories. Those with a significant downwards movement of the end-effector profit from gravitational effects. This profit increases with greater moment of inertia, as the mass of robot links induce a joint torque in the direction of movement and, therefore, lower the share of overall joint torques provided by the motors. Finally, the minimum could be a long distance away from initial trajectory, resulting in a great detour and no improvement in performance. However, non-linear constraints can prevent this problem. In this paper, the exemplary single via-point is kept inside a tube around the initial trajectory, as shown in Figure 12. This constraint is implemented by calculating the via-point's distances in workspace to all points of the initial trajectory. The minimum of these distances is the via-point's distance to the trajectory and it must not exceed the tube radius. Besides, it allows not only a radial shift of the via-point, but in any three dimensional direction.

Experimental Results

The aforementioned approach is applied to the trajectories previously considered in this paper. To avoid the problem of excessive detours, an additional non-linear constraint is implemented. This constraint keeps the optimized via-point inside a tube with a radius of $r = 0.3\text{m}$ around the initial trajectory. However, this only represents a possible first solution

for the problems pointed out before and the settings of that constraint also depend robot and trajectory characteristics. The optimized via-points for each trajectory are presented in Table 3, associated energy and time savings are listed in Table 4. Minimizing the moment of inertia in via-point configuration has shown time savings up to 9.6 % and energy savings up to 6.3 %. Initial and optimized trajectory T3 in workspace are shown in Figure 12. Although this approach cannot set a specific target, it requires less information of the system and significantly lowers computational time of the optimization.

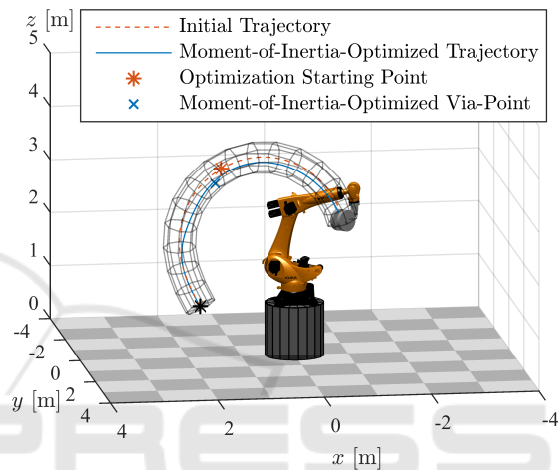


Figure 12: Initial and Moment of Inertia Optimized Trajectory T3.

Table 3: Start and End Configurations of the PTP Trajectories with their Moment of Inertia Optimized Via-Points.

T1	$\mathbf{q}_s^T = [$	0.0	-5.0	0.0	0.0	0.0	0.0
	$\mathbf{q}_{via,in}^T = [$	-0.0	-63.1	-50.0	28.6	-50.0	-6.8
	$\mathbf{q}_e^T = [$	0.0	-140.0	0.0	0.0	0.0	0.0
T2	$\mathbf{q}_s^T = [$	-150.0	-5.0	-90.0	-45.0	-50.0	-45.0
	$\mathbf{q}_{via,in}^T = [$	0.1	-49.1	-0.90	1.8	151.7	170.0
	$\mathbf{q}_e^T = [$	-150.0	-90.0	90.0	180.0	125.0	120.0
T3	$\mathbf{q}_s^T = [$	-55.0	-5.0	10.0	100.0	10.0	-40.0
	$\mathbf{q}_{via,in}^T = [$	-20.0	-55.0	-25.0	-6.6	150.0	100.0
	$\mathbf{q}_e^T = [$	15.0	-105.0	-60.0	-180.0	100.0	50.0
T4	$\mathbf{q}_s^T = [$	165.0	-115.0	-110.0	-316.0	-114.0	-316.0
	$\mathbf{q}_{via,in}^T = [$	0.5	-62.0	0.5	2.0	-147.4	-0.1
	$\mathbf{q}_e^T = [$	166.0	-9.0	111.0	319.0	115.0	319.0

The results show that the approach of reducing moment of inertia is more suitable to optimize trajectories' travel time at this stage. To obtain optimal configuration concerning moment of inertia, given the previously mentioned constraints, major additional axes motion is necessary. This may lead to higher energy demand, e. g. for trajectories T1 and T2. However, T3 and T4 show that further development

may enable to optimize energy consumption and travel time simultaneously. Furthermore, the reduced complexity cost function favors the possibility of online application. Suitable constraints to develop this approach need to be addressed in future works.

Table 4: Results for Moment of Inertia Optimized Exemplary Trajectories.

	Travel Time [s]	Energy Consumption [J]
T1 _{init}	2.96	9733
T1 _{opti.in}	2.78 (- 6.1 %)	10394 (+ 6.8 %)
T2 _{init}	3.50	15005
T2 _{opti.in}	3.20 (- 8.6 %)	16193 (+ 7.9 %)
T3 _{init}	3.01	11769
T3 _{opti.in}	2.72 (- 9.6 %)	11021 (- 6.4 %)
T4 _{init}	4.84	30268
T4 _{opti.in}	4.57 (- 5.6 %)	28492 (- 5.9 %)

ACKNOWLEDGEMENTS

The authors would like to thank the KUKA Roboter GmbH for granting us access to their laboratories to perform power measurements on a KUKA KR 210.

REFERENCES

- (2016). World record: 248.000 industrial robots revolutionising the global economy. IFR press release.
- Biagiotti, L. and Melchiorri, C. (2008). *Trajectory Planning for Automatic Machines and Robots*. Springer Science & Business Media.
- Bobrow, J. E. (1988). Optimal Robot Plant Planning Using the Minimum-Time Criterion. *IEEE Journal on Robotics and Automation*, 4(4):443–450.
- Brossog, M., Bornschlegl, M., Franke, J., et al. (2015). Reducing the Energy Consumption of Industrial Robots in Manufacturing Systems. *The International Journal of Advanced Manufacturing Technology*, 78(5-8):1315–1328.
- Costantinescu, D. and Croft, E. (2000). Smooth and time-optimal trajectory planning for industrial manipulators along specified paths. *Journal of Robotic Systems*, 17(5):233–249.
- Gattringer, H., Riepl, R., and Neubauer, M. (2013). Optimizing Industrial Robots for Accurate High-Speed Applications. *Journal of Industrial Engineering*, 2013.
- Geering, H. P., Guzzella, L., Hepner, S. A., and Onder, C. H. (1985). Time-Optimal Motions of Robots in Assembly Tasks. In *Proc. of the IEEE Conf. on Decision and Control*, pages 982–989.
- Gleeson, D., Björkenstam, S., Bohlin, R., Carlson, J. S., and Lennartson, B. (2015). Optimizing Robot Trajectories for Automatic Robot Code Generation. In *Proc. of the IEEE Int. Conf. on Automation Science and Engineering*, pages 495–500. IEEE.
- Gleeson, D., Björkenstam, S., Bohlin, R., Carlson, J. S., and Lennartson, B. (2016). Towards Energy Optimization Using Trajectory Smoothing and Automatic Code Generation for Robotic Assembly. *Procedia CIRP*, 44:341–346.
- Hamon, P., Gautier, M., and Garrec, P. (2010). Dynamic Identification of Robots With a Dry Friction Model Depending on Load and Velocity. In *Proc. of the IEEE/RSJ International Conference on Intelligent Robots and Systems*, pages 6187–6193.
- Hansen, C., Eggers, K., Kotlarski, J., and Ortmaier, T. (2015). Concurrent Energy Efficiency Optimization of Multi-Axis Positioning Tasks. In *Proc. of the IEEE Int. Conf. on Industrial Electronics and Applications*, pages 518–525.
- Hansen, C., Kotlarski, J., and Ortmaier, T. (2013). Path Planning Approach for the Amplification of Electrical Energy Exchange in Multi Axis Robotic Systems. In *Proc. of the IEEE Int. Conf. on Mechatronics and Automation*, pages 44–50.
- Hansen, C., Öltjen, J., Meike, D., and Ortmaier, T. (2012). Enhanced Approach for Energy-Efficient Trajectory Generation of Industrial Robots. In *Proc. of the IEEE Int. Conf. on Automation Science and Engineering*, pages 1–7.
- Hussong, A. and Heimann, B. (2007). Restricted Minimum-Effort Motion Planning for serial Manipulators. In *Proceedings of the 12th IFToMM World Congress*.
- Johnson, C. T. and Lorenz, R. D. (1992). Experimental identification of friction and its compensation in precise, position controlled mechanisms. *IEEE Transactions on Industry Applications*, 28(6):1392–1398.
- Meike, D., Pellicciari, M., and Berselli, G. (2014). Energy Efficient Use of Multirobot Production Lines in the Automotive Industry: Detailed System Modeling and Optimization. *IEEE Transactions on Automation Science and Engineering*, 11(3):798–809.
- Meike, D. and Ribickis, L. (2011). Industrial Robot Path Optimization Approach with Asynchronous Fly-By in Joint Space. In *Proc. of the IEEE International Symposium on Industrial Electronics*, pages 911–915.
- Mohammed, A., Schmidt, B., Wang, L., and Gao, L. (2014). Minimizing Energy Consumption for Robot Arm Movement. *Procedia CIRP*, 25:400–405.
- Paes, K., Dewulf, W., Vander Elst, K., Kellens, K., and Slaets, P. (2014). Energy Efficient Trajectories for an Industrial ABB Robot. *Procedia CIRP*, 15:105–110.
- Pellicciari, M., Berselli, G., Leali, F., and Vergnano, A. (2013). A method for reducing the energy consumption of pick-and-place industrial robots. *Mechatronics*, 23(3):326–334.
- Riazi, S., Bengtsson, K., Wigström, O., Vidarsson, E., and Lennartson, B. (2015). Energy Optimization of Multi-Robot Systems. In *Proc. of the IEEE Int. Conf. on Automation Science and Engineering*, pages 1345–1350.

- Vergnano, A., Thorstensson, C., Lennartson, B., Falkman, P., Pellicciari, M., Leali, F., and Biller, S. (2012). Modeling and Optimization of Energy Consumption in Cooperative Multi-Robot Systems. *IEEE Transactions on Automation Science and Engineering*, 9(2):423–428.
- Wigstrom, O., Lennartson, B., Vergnano, A., and Breitholtz, C. (2013). High-Level Scheduling of Energy Optimal Trajectories. *IEEE Transactions on Automation Science and Engineering*, 10(1):57–64.
- You, W., Kong, M., and Sun, L. (2011). Optimal Motion Generation for Heavy Duty Industrial Robots Control Scheme and Algorithm. In *Proc. of the IEEE Int. Conf. on Mechatronics*, pages 528–533.

